PTEP

Prog. Theor. Exp. Phys. **2012**, 02B004 (20 pages)
DOI: 10.1093/ptep/pts071

Beam commissioning and operation of the J-PARC main ring synchrotron

Tadashi Koseki[1]*, Yoshitugu Arakaki[1], Yong Ho Chin[1], Keigo Hara[1], Katsushi Hasegawa[1], Yoshinori Hashimoto[1], Yoichiro Hori[1], Susumu Igarashi[1], Koji Ishii[1], Norihiko Kamikubota[1], Takuro Kimura[1], Kunio Koseki[1], Kuanjyun Fan[1], Chikashi Kubota[1], Yuu Kuniyasu[1], Yoshinori Kurimoto[1], Seishu Lee[1], Hiroshi Matsumoto[1], Alexander Molodozhentsev[1], Yuichi Morita[1], Shigeru Murasugi[1], Ryotaro Muto[1], Fujio Naito[1], Hidetoshi Nakagawa[1], Shu Nakamura[1], Kazuaki Niki[1], Kazuhito Ohmi[1], Chihiro Ohmori[1], Masashi Okada[1], Katsuya Okamura[1], Takao Oogoe[1], Kazufumi Ooya[1], Kenichi Sato[1], Yoichi Sato[1], Yoshihiro Sato[1], Kenichirou Satou[1], Masayuki Shimamoto[1], Masashi Shirakata[1], Hirohiko Someya[1], Takuya Sugimoto[1], Junpei Takano[1], Yasuhiro Takeda[1], Yoichi Takiyama[1], Masaki Tejima[1], Makoto Toda[1] Masahito Tomizawa[1], Takeshi Toyama[1], Masahiko Uota[1], Shuei Yamada[1], Noboru Yamamoto[1], Eiichi Yanaoka[1], Masahito Yoshii[1], Hiroyuki Harada[2], Shuichiro Hatakeyama[2], Hideaki Hotchi[2], Masahiro Nomura[2], Alexander Schnase[2], Taihei Shimada[2], Fumihiko Tamura[2], Masanobu Yamamoto[2] and Tetsushi Shimogawa[3]

[1]*KEK, High Energy Accelerator Research Organization, Tsukuba, Ibaraki 305-0801, Japan*
[2]*JAEA, Japan Atomic Energy Agency, Tokai, Ibaraki 319-1995, Japan*
[3]*Department of Physics, Saga University, Honjo, Saga 840-8502, Japan*
*E-mail: tadashi.koseki@kek.jp

Received September 29, 2012; Accepted November 9, 2012; Published December 21, 2012

The slow cycling main ring synchrotron (MR) is located the furthest downstream in the J-PARC accelerator cascade. It became available for user operation in 2009 and provides high-intensity 30 GeV proton beams for various experiments on particle and nuclear physics. The MR has two beam extraction systems: a fast extraction system for beam delivery to the neutrino beam line of the Tokai-to-Kamioka (T2K) experiment and a slow extraction system for beam delivery to the hadron experimental hall. After a nine-month beam shutdown during the recovery from the Great East Japan Earthquake, the J-PARC facility resumed beam operation in December 2011. The MR delivers a 160–200 kW beam to the T2K experiment and a 3.5–6 kW beam to users in the hadron experimental hall. In this paper, a brief review of the MR and the recent status of beam operation are presented. Near-future plans for a beam intensity upgrade are also discussed.

1. Introduction

The J-PARC accelerator is comprised of an H^- linac, a rapid-cycling synchrotron (RCS), the MR and related experimental facilities. The RCS provides a 3-GeV proton beam to the materials and life science experimental facility (MLF) at a repetition rate of 25 Hz. Part of the beam extracted from the RCS is injected into the MR, which accelerates the beam up to 30 GeV before delivering it to the hadron experimental hall (HD) and to a neutrino (NU) beam line, with repetition rates of 0.17–0.4 Hz.

The MR is the furthest downstream and physically the largest accelerator at J-PARC. The layout of the MR and associated experimental facilities is shown in Fig. 1. The MR has a three-fold symmetry

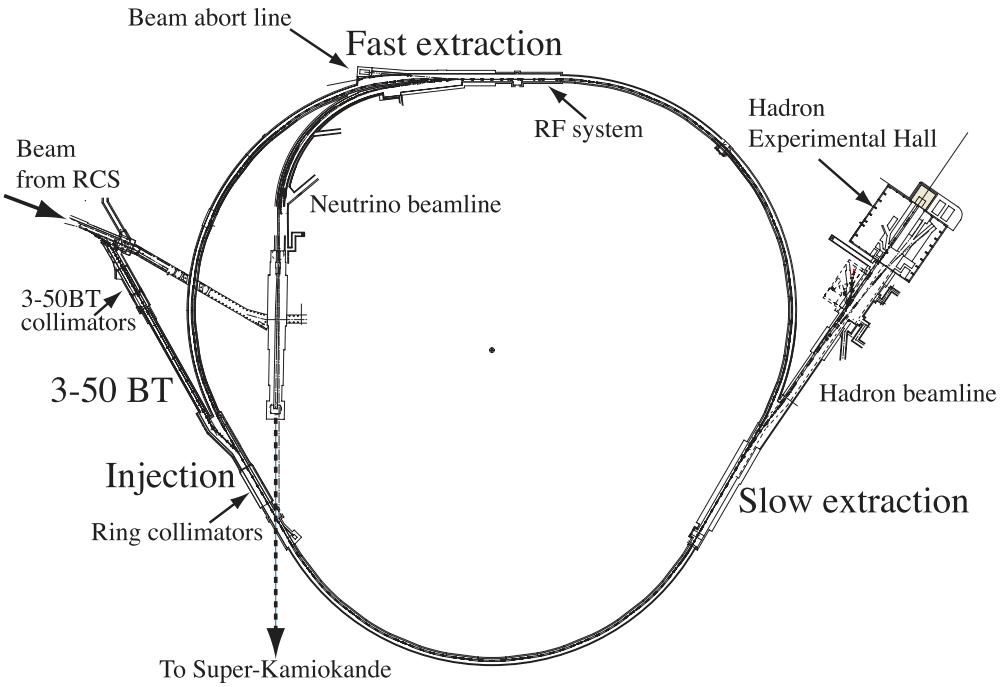

Fig. 1. Layout of the MR and the associated experimental facilities, the hadron experimental hall, and the neutrino beam line.

and a circumference of 1567.5 m. Three 116-m-long straight sections are dedicated to "injection and beam collimators", "slow extraction", and "rf cavities and fast extraction". The slow extraction (SX) system delivers the beam to the hadron experimental hall using third-integer resonance extraction. The fast extraction (FX) system delivers the beam to the neutrino beam line using fast-kicker magnets, which extract all of the beam bunches within a one-turn time period.

The beam from the RCS is divided into two beam transport lines by a pulse bending magnet. Typically 93–97% of the beam (depending on the MR cycle time) goes to the muon and neutron targets in the MLF through the 3NBT which is the beam transport line from the RCS to the MLF. The rest of the beam goes to the MR through the 3-50BT transport line connecting the RCS to the MR. In user operation, two bunches from the RCS are injected into the MR four times and then those eight bunches are accelerated up to 30 GeV.

2. Overview of the MR

The main parameters of the MR are summarized in Table 1. The MR is the first large proton accelerator that adopts an imaginary-transition energy lattice [1]. At the transition energy, the synchrotron oscillation period becomes infinite and there is no phase focusing. Over the years, various ideas and techniques have been tried at many proton synchrotrons in attempting to avoid beam instabilities and associated beam losses that can occur when the acceleration cycle crosses the transition energy. The lattice design of the MR causes it to have an imaginary transition energy. Thus the MR has no transition crossing anywhere between the injection and extraction energies. The transition energy γ_t and momentum compaction factor α are given by

$$\frac{1}{\gamma_t^2} = \alpha = \frac{1}{L}\oint \frac{\eta(s)}{\rho(s)} ds, \tag{1}$$

Table 1. The main parameters of the MR.

Circumference [m]	1567.5
Superperiodicity	3
Typical cycle time for FX [s]	2.56
Typical cycle time for SX [s]	6.0
Injection energy [GeV]	3
Extraction energy [GeV]	30
Harmonic number	9
Number of bunches	8
Typical transition gamma	j31
Physical aperture [π mm-mrad]	$>$81
Collimator aperture [π mm-mrad]	54–81
Number of bending magnets	96
Number of quadrupole magnets	216
Number of sextupole magnets	72
rf frequency [MHz]	1.67–1.72
Number of rf systems	9

where $\eta(s)$ is the dispersion function, $\rho(s)$ is the orbit radius at the orbit position s, and L is the circumference of the ring. By making the momentum compaction negative the transition energy becomes imaginary.

Figure 2 shows the beta function and dispersion of one arc module of the MR. It consists of three FODO cells In the center of the arc module, there is a cell without a bending magnet which is called the "missing bend cell". The dispersion function has a peak value at the missing bend cell and has negative values at both ends of the arc module. This dispersion modulation gives a negative momentum compaction and therefore an imaginary transition energy. Figure 3 shows the beta function and dispersion for 1/3 of the MR. An arc section consists of eight three-FODO arc modules. The 116-m-long straight section consists of three FODO cells and matching sections to the arcs at both ends. The straight section is designed dispersion-free to accommodate the beam collimation, beam injection and extraction systems. The matching section has a large horizontal beta function for injection and extraction septa.

The MR has 96 bending magnets, 216 quadrupole magnets in 11 families, 72 sextupole magnets in 3 families and 186 steering magnets (93 each for the horizontal and vertical directions). All the magnets are excited by IEGT/IGBT-based power supplies. For the rf system, a design with high gradient broadband cavities using magnetic alloy (MA) cut-cores has been adopted [2]. Currently there are nine rf systems. For beam injection, a one-turn injection method has been adopted. Bunches received through 3-50 BT are delivered into the MR by the injection system, which is composed of two injection septa, four injection kickers and three injection-bump magnets. Downstream of the injection system, there is a ring collimator section which scrapes off the beam halo and consequently localizes the beam losses to the collimator section. The ring collimator section was originally designed to handle losses up to 0.45 kW. This capacity has been increased to 2 kW by installing additional collimator units in 2012. In addition, there is another collimator section in 3-50 BT. The 3-50 BT collimator section itself has a loss capacity of 2 kW upgraded from 0.45 kW to the present 2 kW by installing additional iron shields in the 2010 summer shutdown. At this collimator section, the halo of the beam extracted from the RCS is eliminated before MR injection.

The FX system is composed of five kicker magnets and six septum magnet systems. The rise time of the kicker is $\sim$1 μs and all the circulating bunches are extracted within $\sim$5 μs. Two of the septum magnets, SM1 and SM2, are of a low field strength type ($\sim$0.26 T for extraction of 30 GeV beam) and the remaining four septum magnets, SM30–33, are of a high field strength type (0.96–1.1 T for

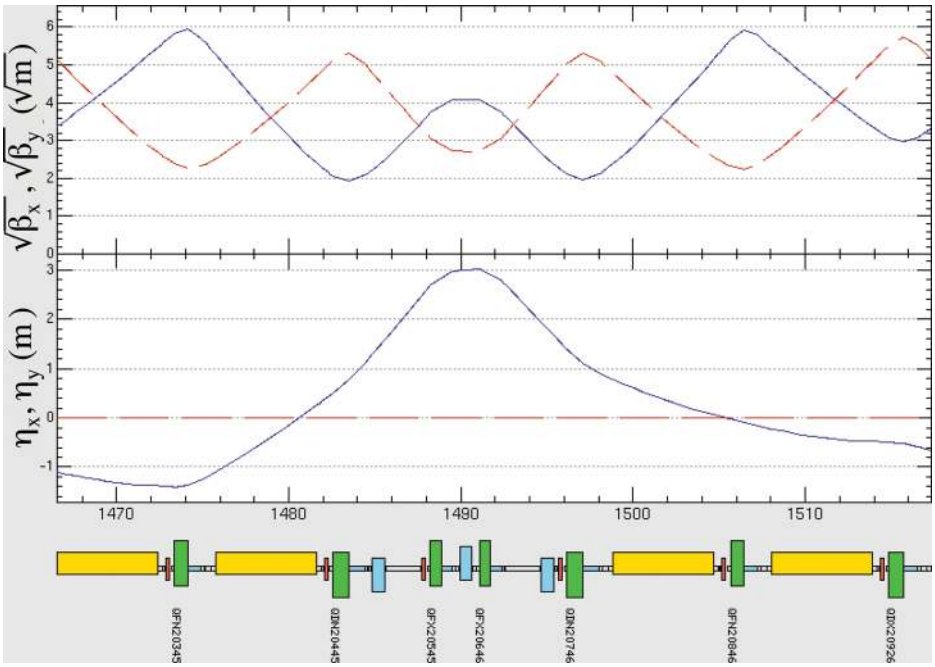

Fig. 2. Beta (β_x, β_y) and dispersion (η_x, η_y) for the unit cell of the MR arc section. Blue and red lines show values for the horizontal and vertical directions, respectively.

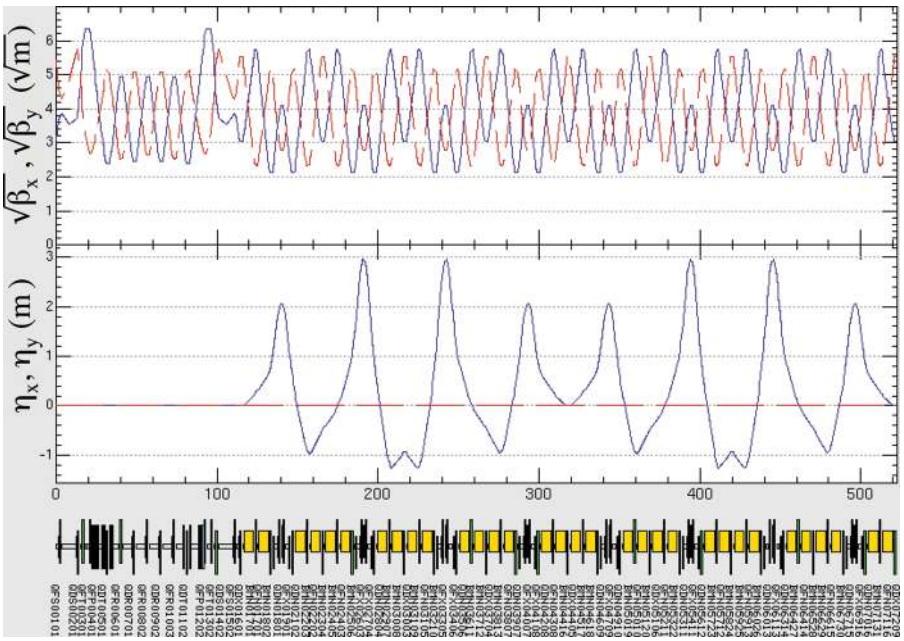

Fig. 3. Beta (β_x, β_y) and dispersion (η_x, η_y) for one of the symmetric 1/3 sections of the MR. Notation of the lines are the same as Fig. 2.

extraction of 30 GeV). All the kickers and septa are bipolar system and can bend the extraction beam away from the ring both inside (to the neutrino beam line) and outside (to the abort beam line).

Figure 4 shows a plan view of the SX straight section. The SX system [3] has four bump magnets (SBMP1–SBMP4), two electrostatic septum deflectors (ESS1&2), ten magnetic septa (SMS1-1 & SMS1-2, SMS2-1–SMS2-4, SMS3-1–SMS3-4) in a straight section, which is then connected by a beam transfer line to the hadron experimental facility. Eight sextupole magnets are located in the arc

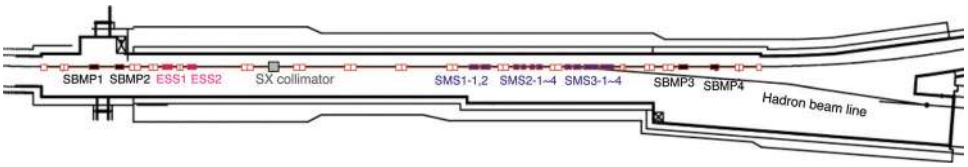

Fig. 4. Straight section dedicated to the SX system.

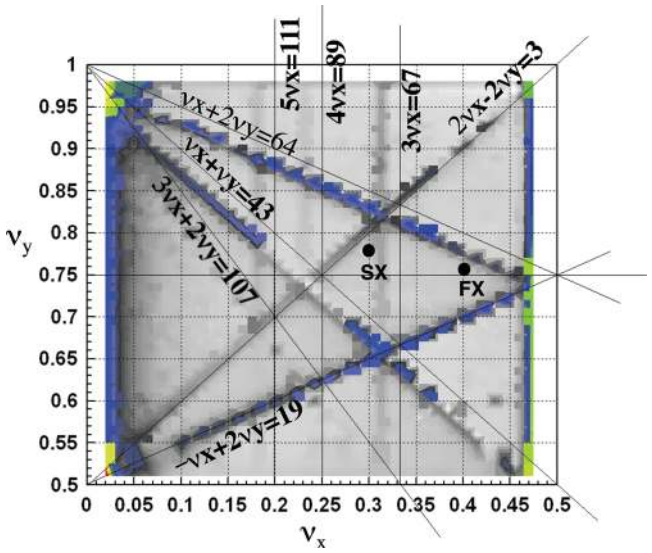

Fig. 5. Result of aperture survey and operating points for FX and SX operations.

sections in order to excite a third-integer resonance, $3\nu_x = 67$. After the beam is accelerated up to 30 GeV, the horizontal tune is ramped up to the resonance line by changing one of the quadrupole families, QFN, which has 48 magnets located in the arc sections. An SX collimator was installed during the 2011 shutdown period to absorb stray protons, which are scattered by the ESS ribbons with the aim of decreasing residual radioactivity on the downstream quadrupole magnet. The beam power available is restricted by the beam loss in the extraction areas. The β_x at the first ESS position is designed to 40 m, the highest value in the ring. As a result of this large β_x, the step size, which is the horizontal position difference at the ESS between the extracted beam and the beam position three turns before, is ∼20 mm. This large step size contributes to the low rate of beam impacting on the ESS septum.

Figure 5 shows a tune diagram of the MR. It is a simulation result of a beam survival study for an on-momentum single particle [4]. In this simulation, the measured imperfections of the magnets such as field errors, alignment errors and higher-order field components of the bending, quadrupole and sextupole magnets, and the fringe-field effect of the quadrupole magnets were taken into account. The typical operating tunes for FX and SX operation are also shown in the figure. The operating point for the SX is set close to the third-integer resonance line $3\nu_x = 67$ to perform the resonance extraction.

Figure 6 shows both the FX and SX mode operating profiles of the acceleration cycle magnet currents, as derived from the kinetic energy of the proton beam, and the circulating beam current, as measured by a DC current transformer (DCCT). As the harmonic number of the RCS is two, a two-bunch beam extracted from the RCS is injected into the MR four times with a time interval of

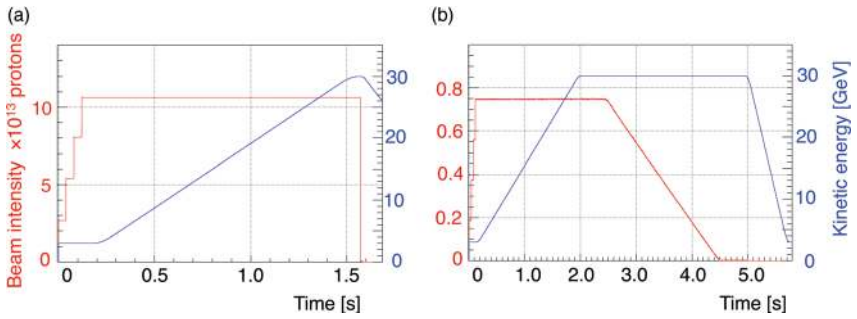

Fig. 6. Intensity and kinetic energy profiles of a typical operation cycle for the (a) FX and (b) SX modes.

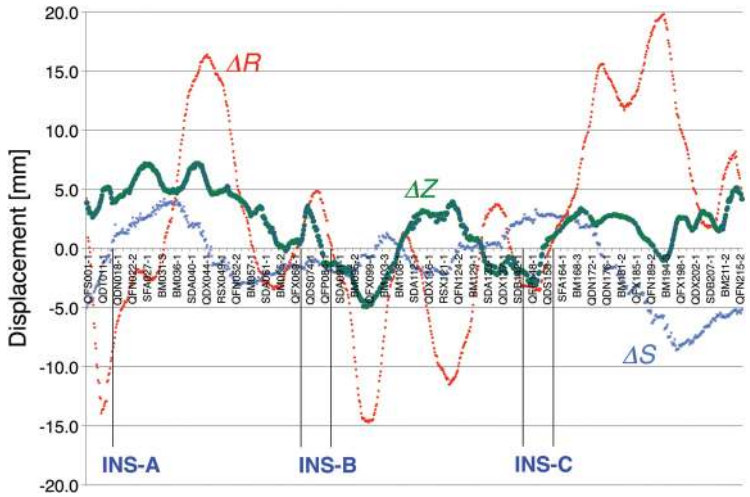

Fig. 7. Measured displacements of MR magnets after the earthquake in the horizontal (R), vertical (Z) and longitudinal (S) directions. Labels Ins-A, B, and C indicate the straight sections for "beam injection," "slow extraction," and "RF and fast extraction," respectively.

40 ms (25 Hz). Those eight bunches are then accelerated in the MR from 3 GeV to 30 GeV. Such an acceleration time is less than 2 s. The minimum acceleration time is limited by the main magnet power supply and the rf system, and is 1.4 s at the present. After the energy has been ramped up to 30 GeV, all bunches are extracted by the fast kicker magnets in the FX mode. While in the SX mode, the beam is debunched by switching off the rf power at 30 GeV and then slowly extracted over 2 s by resonant extraction. For this figure, the cycle times and delivered beam powers are 2.56 s and 200 kW for the FX mode and 6.0 s and 6 kW for the SX mode.

3. Recovery from the earthquake and recommissioning of the MR

The J-PARC facility was seriously damaged by the Great East Japan Earthquake on 11 March 2011 [5]. In the MR tunnel, a few tens of cracks were discovered and many of them began leaking groundwater just after the earthquake. The groundwater fell on magnets and vacuum ducts of the MR like rain. Urethane and a high-molecular weight compound cement were used to fill the cracks and stop the water leaks.

Figure 7 shows the magnet positions measured in April and May 2011 using a laser tracker system [6]. The maximum displacements after the earthquake were greater than ±15 mm horizontally and 10 mm peak-to-peak vertically. We realigned all the magnets and most of the monitors in the ring during the shutdown from the end of August to the beginning of December 2011.

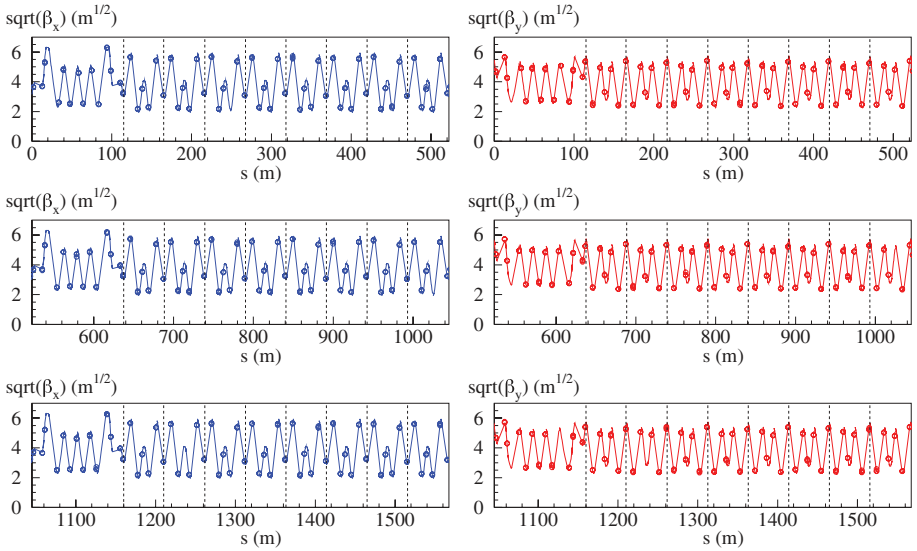

Fig. 8. β_x (left) and β_y (right) around the whole ring. Designed and measured values are presented by a solid line and circles, respectively.

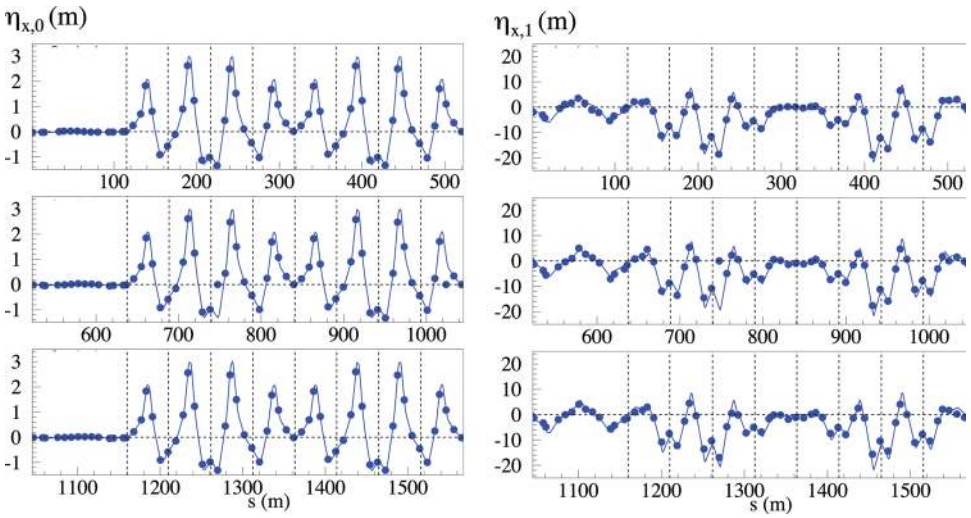

Fig. 9. Linear (left) and nonlinear firstorder (right) dispersion η_x around the whole ring. Designed and measured values are presented by a solid line and circles, respectively.

The J-PARC facility resumed beam operation in December 2011. Transport of a beam with nominal energy but at a low intensity of 4×10^{11} particles per bunch (ppb) from the linac to the targets in MLF and neutrino beam line was successfully demonstrated in December 2011. In January 2012 normal user operation resumed [7].

After the initial recovery from the earthquake damage, beam optics parameters were measured at a low beam intensity of 4×10^{11} ppb. Figures 8 and 9 show comparisons between the designed and measured values of β_x, β_y, and η_x around the whole ring. The measured values are for the data taken after the optics correction, in which correction factors for all eleven quadrupole power supplies were determined by fitting to reproduce the designed β, η, and betatron tunes [8,9]. The measured parameters after the optics correction agree well with the design expectation. Figure 10 shows the measured horizontal and vertical chromaticities (momentum dependence of the horizontal

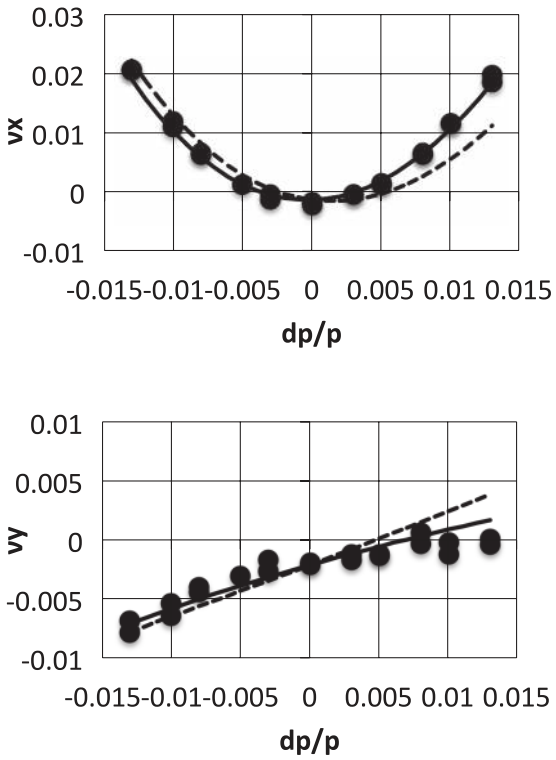

Fig. 10. The *dp/p* dependence of the horizontal (top) and vertical (bottom) tunes. The closed circles show the measured results. The solid and dashed lines show calculation results with and without the sextupole component of the bending magnets taken into account.

and vertical betatron tunes) after chromaticity correction using the 72 sextupoles [9]. The solid and dashed curves in the figure show calculated results with and without taking into account measured sextupole components in the bending magnets. Although the sextupole component in each bending magnet is small, it is not negligible over the total 96 bending magnets. The calculation taking into account their sextupole components gives better agreement with the measurements.

The optics measurements performed in the recommissioning run just after the earthquake recovery match the design well. After completing this tuning at low intensity, we gradually increased the beam power to be able to go back into user operation.

4. High power operation for the T2K experiment

4.1. Beam power upgrade history

The T2K experiment started taking physics data in January 2010. Figure 11 shows the history of the beam power delivered from January 2010 to the last day of operation before the 2012 summer shutdown. For the FX mode, the beam power was increased by shortening the acceleration cycle time as shown in Fig. 11, and by increasing the number of extracted particles per pulse. The shortening of cycle time was achieved by improvements to the main magnet power supplies and installation of additional rf systems to attain a higher accelerating power. The number of the rf systems was five until June 2010. A 6^{th} system was installed during the 2010 shutdown, the 7^{th} and 8^{th} during the 2011 shutdown and finally the 9^{th} during the 2012 shutdown.

In the period up until June 2010, the beam power was limited by the performance of the FX kicker, which had a slow rise time of 1.6 μs and a problem with kick angle drift [10]. The 1.6 μs rise time

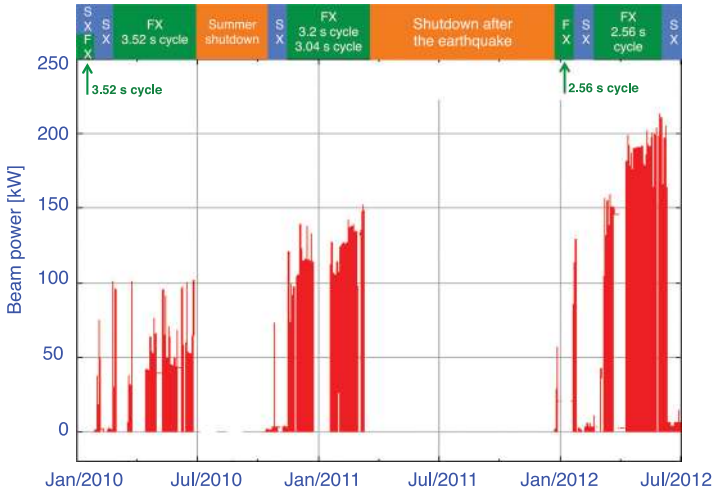

Fig. 11. History of the MR output beam power. The extraction mode in each period is also shown.

limited the maximum number of circulating bunches in the MR to be six. The problem of kick angle drift was due to heating of the ferrite cores from the beam-induced field. This occurred during continuous operation when the beam power was greater than 50 kW. During the 2010 summer shutdown, all five kickers were replaced with newly developed ones, which have a rise time of less than 1 μs [10]. This made operation with eight bunches possible, which was the original design bunch configuration for the MR. The new kicker system also has damping resistors to reduce the beam coupling impedance, along with cooling water channels on the ferrite cores.

Beginning in November 2010, the bunch-by-bunch feedback system was switched on [11]. The bunch-by-bunch feedback system effectively suppressed the transverse coherent oscillation and reduced beam loss. The delivered beam power reached 145 kW before the long shutdown in the aftermath of the earthquake.

After the earthquake, restoration work on the damage caused by the earthquake and some improvements were made during the nine-month shutdown period of 2011. The injection kicker magnets were replaced with newly fabricated ones during this period [12]. The traveling-wave-type injection kickers used until March 2011 had problems of discharging in a vacuum chamber as well as high beam-coupling impedance. The new kickers have a simple lumped-impedance-type structure, a well-shaped driving pulse waveform, and a lower beam-coupling impedance. After the nine-month shutdown, beam operation of the MR resumed in December 2011. Beam delivery to the T2K experiment was restarted in March 2012 and the beam power achieved before the earthquake was reattained in the middle of the same month. In May 2012, the rf feed-forward system for beam loading compensation was turned on for user operation (F. Tamura et al., manuscript in preparation). The feed-forward system reduced the beam loss occurring at the beginning of the acceleration cycle. The maximum delivered beam power was increased to 200 kW in June 2012.

Figure 12 shows the history of the beam delivered to the T2K experiment from the start of the physics data taking to the morning of 9 June 2012, which was the last day of delivering beam to the T2K experiment before the 2012 summer shutdown. The number of protons on target (POT) for each day and the integrated POT are plotted (data courtesy of the T2K group). The total delivered number before the earthquake was 1.43×10^{20} and the grand total number at present is 3.1×10^{20} POT. On 15 June 2011, the T2K group announced that the T2K experiment had detected six electron

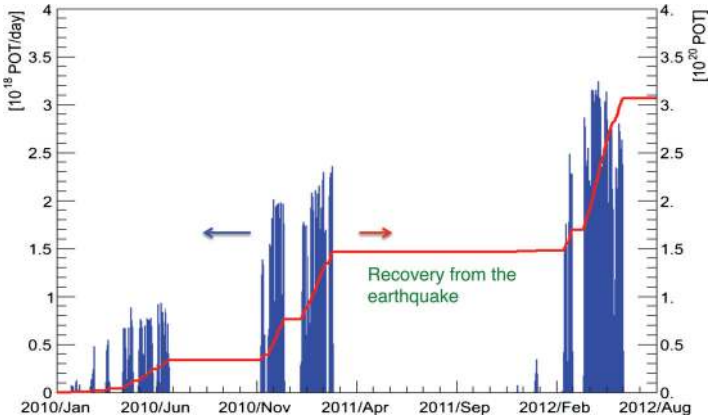

Fig. 12. History of delivered proton count to the T2K experiment.

neutrino candidate events based on the data collected before the earthquake. For the first time, it indicated that muon neutrinos are able to transform into electron neutrinos over the 295 km distance through neutrino flavor oscillation [13]. By using all the date taken until the present, the number of possible electron neutrino candidate events has been increased to eleven. The T2K group work shows evidence for the appearance of electron neutrinos with a statistical significance of 3.2σ.

4.2. Key issues for high power operation

For operation at a high beam power, a bunch-by-bunch feedback system is critically important. In the MR, coherent oscillation of the betatron sideband is observed in routine user operation. The instability is due to the resistive wall impedance of the stainless-steel beam-duct and the beam-coupling impedance of the injection and extraction kickers [14]. In addition, the field of the present injection kicker system affects the circulating beam and may cause oscillation in the horizontal direction. Since the natural chromaticity of the MR is a large negative value of -30, the instability can be suppressed by controlling the chromaticity. In fact, both horizontal and vertical chromaticities are set to be between -1 and -5 to suppress instability in user operation. However, the damping effect of a negative chromaticity of ~ -5 is not sufficient for high power beam operation with beam intensities greater than $\sim 5 \times 10^{13}$ particles per pulse (ppp). Therefore, a bunch-by-bunch feedback system is necessary for stable user operation with even higher intensity beams.

Figure 13 shows a block diagram of the bunch-by-bunch feedback system [11]. The beam position monitor (BPM) detects the coherent bunch motion in both the horizontal and vertical directions. The waveform signal is fed into a digital processing circuit, which has four 14-bit ADCs (analog to digital converters), an FPGA (field-programmable gate array), and two 14-bit DACs (digital to analog converters). The signal processing circuit extracts the betatron oscillation signal using an 8-tap FIR (finite impulse response) filter and calculates the feedback value output. The signal is sent to strip-line kickers through power amplifiers. The kicker kicks the corresponding bunch to suppress the oscillation. Figure 14 shows the circulating beam intensity measured by a DCCT monitor at 9×10^{13} ppp. The red charts show the results of turning the bunch-by-bunch feedback on (solid curve), and with it off (dotted curve). The blue chart shows the time variation of the kinetic energy of the beam. Figure 15 shows the delta signal from the BPM in the horizontal direction for the same shots as shown in Fig. 14. Without the feedback, a large oscillation occurred just after the acceleration started and half of the particles were lost. In contrast, with feedback the beam is stably accelerated

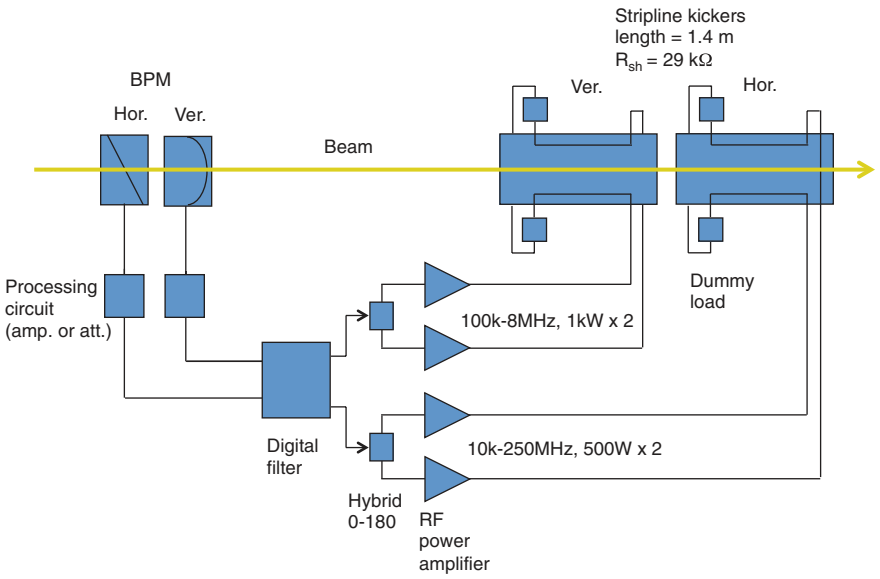

Fig. 13. Block diagram of the bunch-by-bunch feedback system [11].

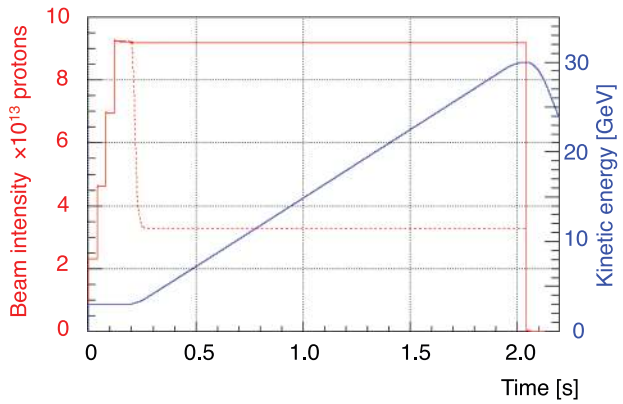

Fig. 14. Measured circulating beam intensity with (red solid curve) and without (red dotted curve) bunch-by-bunch feedback. The blue chart shows the time variation of the kinetic energy of the beam.

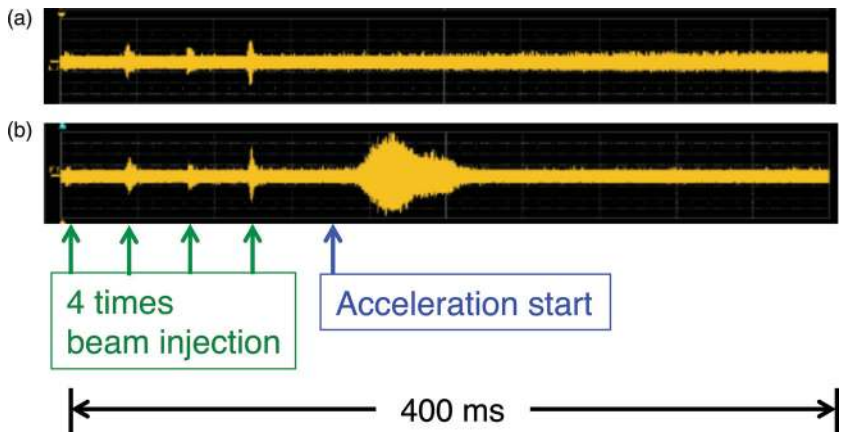

Fig. 15. Delta signal from the BPM in the horizontal direction with (a) and without (b) bunch-by-bunch feedback.

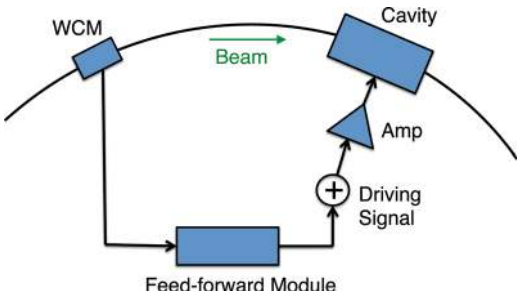

Fig. 16. Block diagram of the low-level rf feed-forward system [15].

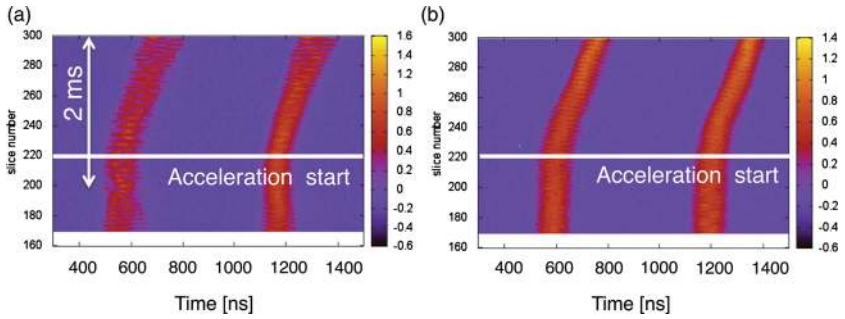

Fig. 17. Mountain plot of WCM signals for two-bunch acceleration without (a) and with (b) feed-forward.

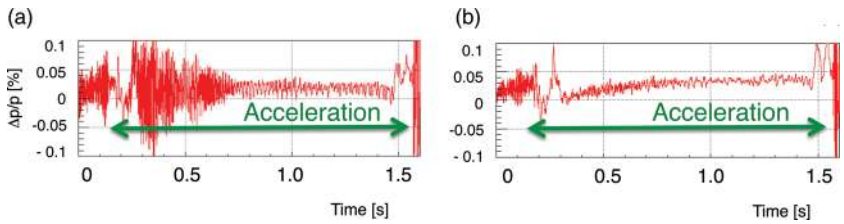

Fig. 18. Time dependence of the averaged momentum deviation measured by BPMs without (a) and with (b) feed-forward.

without any beam losses during acceleration. The bunch-by-bunch feedback has been applied for routine user operation since November 2010.

Another key component for high power operation is an rf feed-forward system for beam loading compensation [15]. The diagram of the feedforward system is shown in Fig. 16. Beam signal picked up by a wall current monitor (WCM) is fed into the feed-forward module of a low-level rf system. The module creates a signal driving an rf cavity that can cancel the cavity wake voltage. Figure 17 shows a mountain plot of the WCM signal for two bunches. Figure 18 shows the time dependence of the averaged momentum deviation, which is calculated using measured position data from all of the BPMs. These two figures show that the large longitudinal oscillation growth during the acceleration is effectively suppressed by the feed-forward system. Suppressing the oscillation reduces beam loss, which had occurred just after the acceleration start. The feed-forward system has been switched on for user operation since May 2012.

Figure 19 shows the distribution of the integrated beam loss monitor (BLM) signals from one shot. The beam intensity is 1.08×10^{14} ppp, which corresponds to 203 kW operation with a 2.56 s cycle time. The horizontal axis gives the ring address of the BLM. With this beam intensity, the

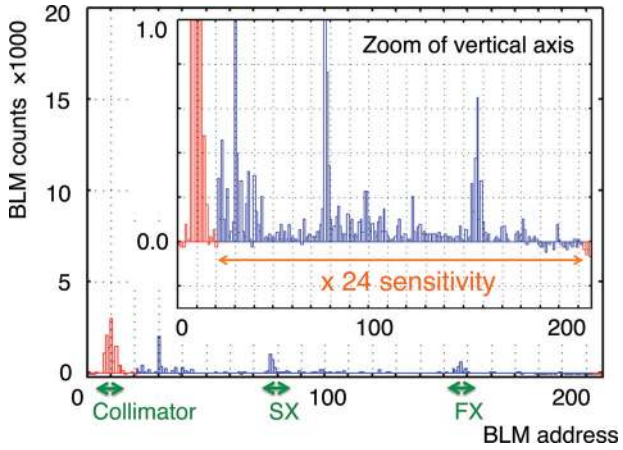

Fig. 19. Distribution of the beam loss monitor signals in high power beam operation of 1×10^{14} ppp. The signal sensitivity of the blue part is 24 times larger than that of the red part.

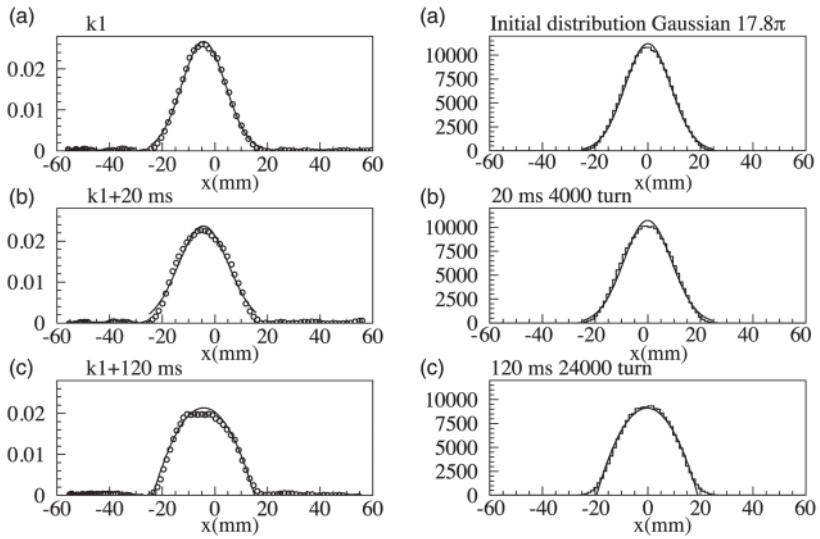

Fig. 20. Measured (left) and simulated (right) horizontal beam profiles during the injection period for a beam intensity of 1×10^{13} ppb at the FX operating point at (a) injection timing k1, (b) k1 + 20 ms, (c) k1 + 120 ms.

number of lost particles is typically 1–2% of the total and most of the beam loss occurs during the injection period and the beginning of the acceleration. Although the beam loss is mostly localized to the collimator section, a small loss is observed downstream of the collimator section and at the ESS in the SX straight section. This remaining beam loss will cause a serious residual radioactivity problem whenever higher beam intensity operation begins in the future. Additional collimator units were installed in the collimator section during the 2012 summer shutdown in order to reduce the beam loss downstream of the collimator section.

Figure 20 shows measured and simulated horizontal beam profiles during the injection period for a beam intensity of 1×10^{13} ppb at the FX operating point. The time dependence of the simulated profiles agrees well with the measured data, which are obtained by a flying-wire profile monitor (FWPM) in the dispersion-free straight section [16]. The incoherent tune shift is ∼0.15 and the profile is thought to be affected by the linear coupling resonance $\nu_x + \nu_y = 43$. Resonance correction using four skew quadrupoles is scheduled for the fall of 2012.

5. Slow extraction

The MR delivered a beam power of 3–6 kW to the hadron experimental facility after the earthquake. In user operation, a dynamic bump scheme was adopted to reduce beam loss in the extraction [3]. Figure 21 shows schematic diagrams of separatrices for the fixed and dynamic bump schemes. The solid and dotted lines show the separatrices at the beginning and end of the extraction, respectively. For the fixed bump scheme, the center of the separatrix is fixed during the extraction and beam angle (dx/ds) at the ESS septum changes between the beginning and end of the extraction. This causes a change in the effective thickness of the septum for the beam and also a change of beam loss between the beginning and end of the extraction. For the dynamic bump scheme, the center of the separatrix is adjusted to fix the beam angle at the ESS septum during the extraction. This can reduce the impact rate of the beam on the ESS septum and beam losses in the downstream magnetic septa.

Figures 22 and 23 show the beam loss distribution in the SX straight section and time dependence of the beam loss for fixed bump operation and dynamic bump operation. The data was taken before the installation of the SX collimator. As can be seen in the figures, the beam loss is drastically reduced in the dynamic bump operation. The extraction efficiency evaluated from the BLM signals for the fixed bump operation is 98.3%, while for dynamic bump operation it is 99.5%, the world's highest extraction efficiency for slow extraction.

As reported elsewhere, the most serious problem to be solved for SX operation is the appearance of a spike-like time structure on the extracted beam [3,17]. This structure arises from fluctuations in the betatron tune, which are due to current ripples, $\Delta I/I \sim 10^{-4}$ of the main magnet power supplies. To improve the time structure, we have adopted a spill feedback system, which consists of two types of fast quadrupoles and a DSP (digital signal processor) control system. Additionally, a "trim coil short" method was implemented to reduce the ripple in the magnetic field [18]. In the MR, all the quadrupoles have a 24-turn main coil and an 11-turn trim coil on each pole. When the trim coil is shunted by a MOSFET relay installed in each trim coil, the ripple components of the main coil current flow into the trim coil and the magnetic field ripple is reduced.

To describe the spill time structure, we define the spill duty factor as

$$Duty = \left(\int_{T1}^{T2} I(t)dt\right)^2 \Big/ \int_{T1}^{T2} dt \int_{T1}^{T2} I(t)^2 dt, \tag{2}$$

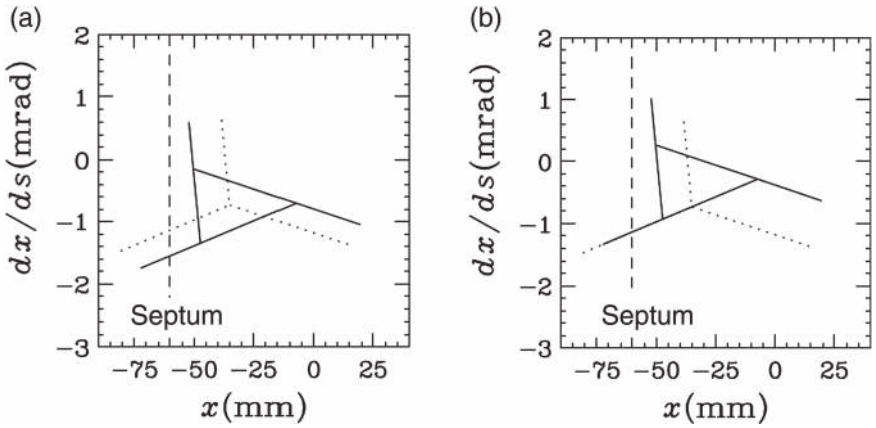

Fig. 21. Schematic diagram of separatrices for fixed (a) and dynamic bump (b) schemes. The solid and dotted lines show the separatrices at the beginning and end of the extraction, respectively.

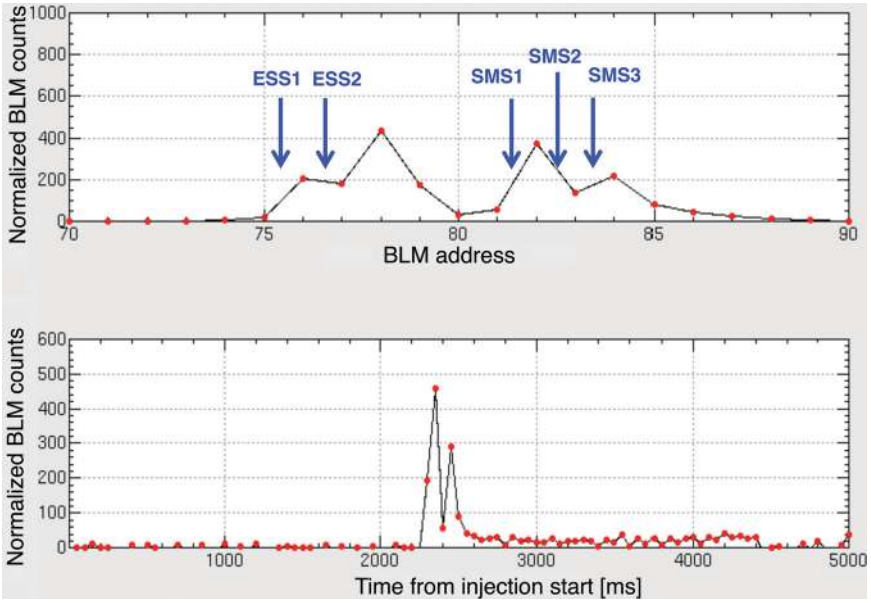

Fig. 22. Beam loss distribution in the SX straight section (top) and time dependence of the beam loss (bottom) for the fixed bump operation.

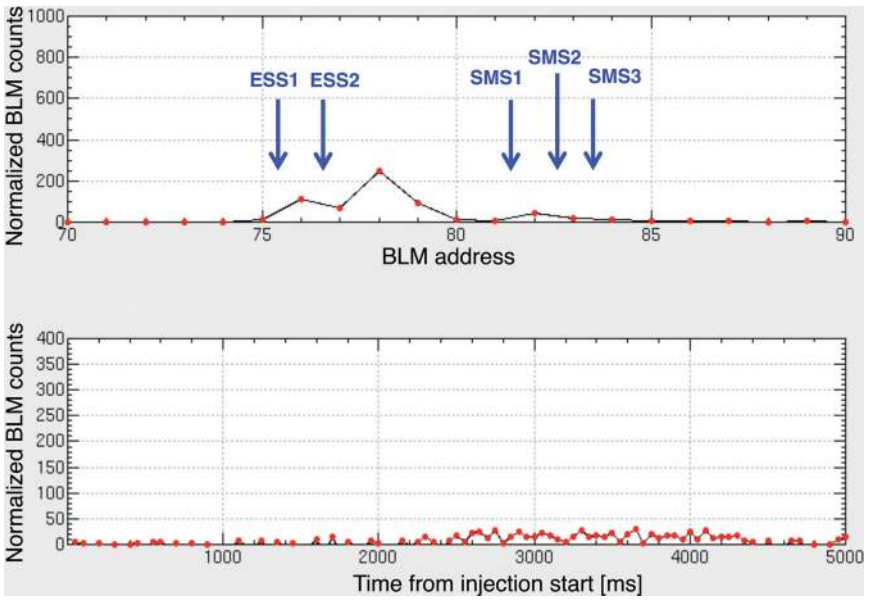

Fig. 23. Beam loss distribution in the SX straight section (top) and time dependence of the beam loss (bottom) for the dynamic bump operation.

where $I(t)$ is the beam spill intensity, and times $T1$ and $T2$ define the gate width. The typical duty factor for user operation before the earthquake was ∼17%; this was measured with the spill feedback on and the trim coil shunts in use. Recently, for further improvement of the duty factor, we have switched on a transverse rf system, which feeds an rf field with a narrow bandwidth around the frequency of the betatron oscillation to a strip-line kicker [19,20]. This increases the amplitude of the oscillation and pushes the beam to the third-order resonance for extraction. In order to suppress the vacuum pressure rise due to the multipactoring effect in the strip-line kicker, 12 sets of solenoid

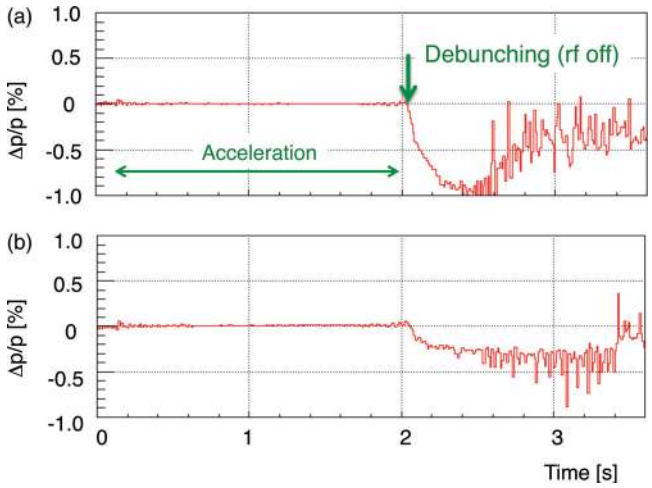

Fig. 24. Averaged $\Delta p/p$ of the circulating beam for 6 kW operation: rf feed-forward off (a) and on (b).

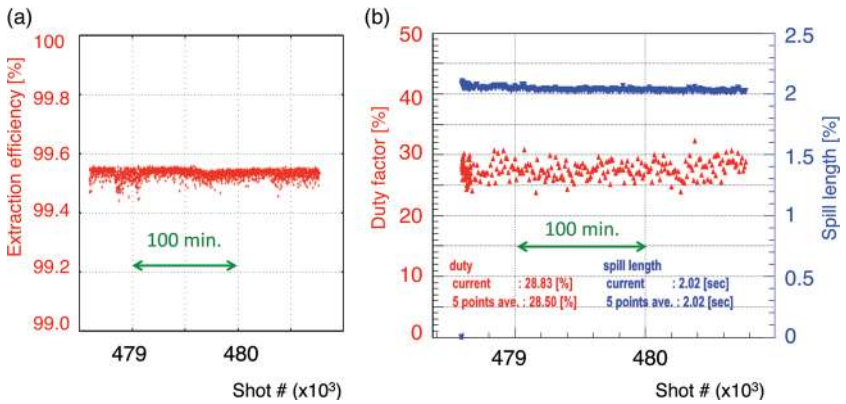

Fig. 25. Time dependence of extraction efficiency (a) and duty factor and spill length (b) during the 6 kW user operation.

coils were installed on the beam duct of the strip-line kicker. Using this transverse rf system, the duty factor during user operation in February 2012 was improved from 17% to 30%.

In user operation, the rf accelerating power is switched off during the extraction in order to deliver a debunched beam to the users. Figure 24(a) shows the time dependence of the averaged $\Delta p/p$ of the circulating beam in 6-kW operation. The beam is decelerated after the debunching (rf off) by the impedance of the ring (mainly the impedance of the rf cavities) and the averaged momentum is reduced during extraction. The deceleration causes a deterioration of the extraction efficiency because the large momentum decrease leads to a tune shift due to the higher-order effect of the chromaticity, as shown in Fig. 10. The deceleration effect becomes larger as the beam intensity becomes larger. An rf feed-forward system was found to be fairly effective in ameliorating the deceleration effect, because it can decrease the beam coupling impedance of the tf cavities to almost zero during the extraction period. Figure 24(b) shows the averaged $\Delta p/p$ with rf feed-forward. The deceleration effect is suppressed by the feed-forward and as a result the $\Delta p/p$ decrease is improved from -1% to -0.3%. The rf feed-forward system was adopted for routine user operation of the SX in June 2012.

Figure 25 shows the time dependence of the extraction efficiency (a), duty factor, and spill length (b) during 6-kW user operation. As can be seen, the efficiency, duty factor, and spill length are held stable during the operation.

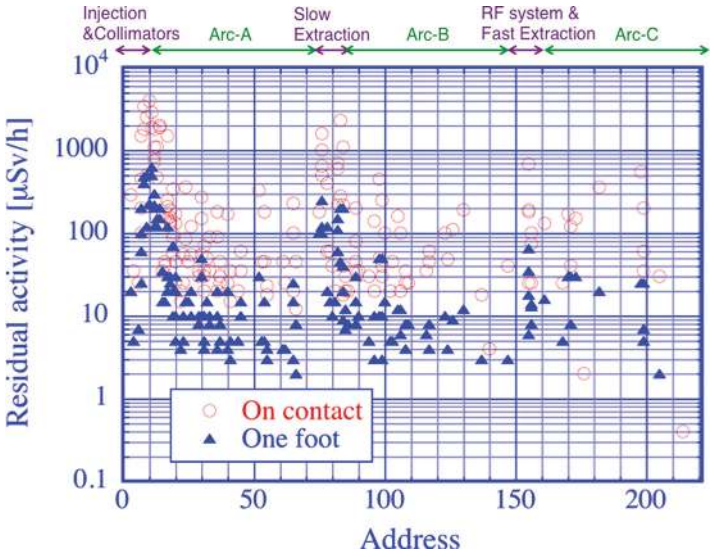

Fig. 26. Residual radioactivity measured at four hours after the beam stop of 6 kW operation in SX mode. The measured residual activity in the ring collimator section is mainly caused by the high power operation of 160–200 kW for the T2K experiment, which had ended one month previously.

Before the 2012 summer shutdown, a maximum extracted intensity of 1.7×10^{13} ppp was successfully demonstrated. This corresponds to a beam power of 14 kW at the 6.0 s cycle operation. The extraction efficiency and duty factor were 99.5% and 33.7%, respectively. After the 2012 shutdown, user operation with beam powers greater than 10 kW will begin.

Figure 26 shows the distribution of the residual radioactivity around the whole of the ring as measured four hours after the beam stop in the 6-kW SX operating mode on 2 July 2012. The red and blue symbols show the data measured on contact and at a one-foot distance. The beam delivery of 160–200 kW for the T2K experiment was stopped on 9 June 2012 and after that the MR continued to deliver beam in the SX mode for about another month. Therefore, we can infer that the measured residual activity in the ring collimator section was mainly due to the high power operation for the T2K experiment and the activity in the SX straight section was caused by the SX operation in July.

6. Future plans

Table 2 shows the calendar for near-term operational planning of the MR for both FX and SX. The 9^{th} rf system installed in 2012 makes it possible to operate one or two rf systems at the second harmonic frequency. The second harmonic system permits manipulating the longitudinal particle distribution in each bunch so as to reduce the effect of space charge forces. The ring collimator system will be improved to increase beam loss capacity from the present 2 kW to 3.5 kW in 2013 by installing additional collimator units and iron shields. In 2013, the J-PARC facility will take a 6-month shutdown to upgrade the linac [21]. During that long shutdown period, the ESSs will be replaced with newly fabricated ones, which will have vacuum chambers made of titanium instead of stainless steel. The titanium chamber is expected to decrease the residual radioactivity of the chambers after slow extraction operations.

The design goal for the MR is to achieve a beam power of 750 kW for FX operation. In the original scenario envisaged just at the beginning of the J-PARC project, it was thought that the design beam power could be accomplished by a beam energy upgrade from 30 GeV to 50 GeV. Accordingly, the

Table 2. Near-term plan of beam intensity upgrade of the FX and SX modes.

	Fast Extraction	Slow Extraction	
July 2012–Sep 2012	Upgrade of ring collimator section	Installation of titanium chambers	
(3-month shutdown)	Installation of 9th rf system	in magnetic septum section	
Oct 2012–June 2013	>200 kW	10 kW	50 kW
	User operation	User operation	Accelerator study
Aug 2013–Jan 2014	Upgrade of ring collimator section	Installation of titanium chambers	
(6-month shutdown)		in ESS section	
Feb 2014–June 2014	>300 kW	50 kW	100 kW
	User operation	User operation	Accelerator study

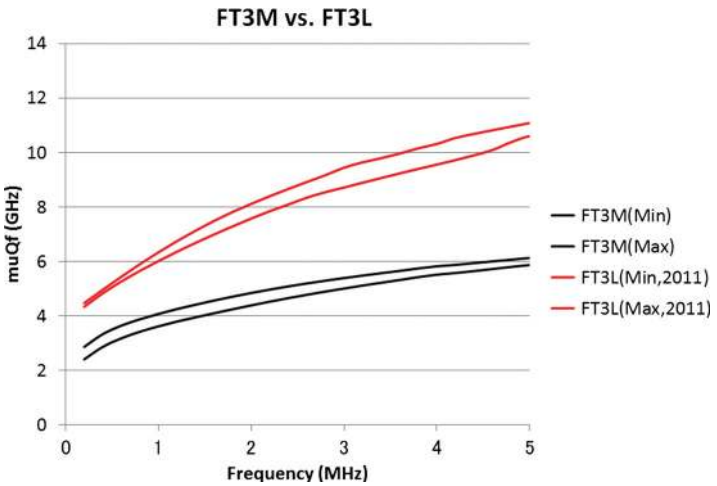

Fig. 27. Measured frequency dependence of μQf values for the FT3M (black curves) and FT3L (red curves) cores. Each pair of curves shows the maximum and minimum values obtained over all of the measured cores.

main magnet system of the MR was designed also assuming a 50-GeV operation. However, magnetic saturation effects on both the bending and quadrupole magnets become significant around the operational currents needed for 50 GeV, and their magnet field qualities are degraded markedly in 50-GeV operation. In addition, the total magnet power needed for 50-GeV operation is approximately four times larger than for 30-GeV operation due to the large saturation effect. The accompanying high electrical energy cost is disadvantageous at any time, but especially now under the conditions after the earthquake disaster because of reduced generation capacity. Instead of increasing the beam energy, a new scenario for achieving the design goal calls for moving toward a higher repetition rate than at present: i.e. from ∼0.4 Hz to ∼1 Hz.

In order to implement the proposed high repetition rate operation scenario, two critical R&D projects are now going on aggressively. The first requirement is for a magnet power supply capable of 1 Hz repetition rate with very low ripple current [22]. The design calls for a large capacitor bank system for energy recovery to improve efficiency and to reduce the variation in input primary power line. For ripple reduction, an NPC (neutral point clamped) chopper has been chosen for the DC–DC converter, as this configuration can reduce common-mode ripple. Also, a digitally controlled current feedback system and a filter working at a switching frequency higher than 10 kHz are being developed to reduce normal-mode ripple.

The second essential R&D project is the development of an rf cavity with a higher field gradient. This can be done by using improved materials, in particular the MA core type, specifically the FT3L made by Hitachi Metals. This product, which is processed by annealing in a magnetic field, shows

higher impedance than FT3M, which is the present core used in the J-PARC synchrotrons [23]. Since the recovery from the earthquake, more than 10 of the fullsize FT3L cores for the rf cavity of the MR have been manufactured at the J-PARC site in collaboration with Hitachi Metals. Figure 27 shows the typical frequency dependence of the μQf value, this figure of merit is the product of permeability, quality factor, and frequency. The measurements were made at a low rf power level, comparing the newly manufactured full-size FT3L cores and the present FT3M cores. The μQf value is proportional to the shunt impedance of the core. The manufactured FT3L cores show an impedance approximately twice that of the FT3M cores. Six of the FT3L cores have been installed in one gap of the tank in the 9$^{\text{th}}$ rf cavity, which was installed during the 2012 summer shutdown. The target year for finishing the hardware upgrades and replacements needed for high-repetition rate operation is 2017, which, however, depends on government approval of the budget.

For the SX operation, the delivered beam power is limited by the beam loss and residual radioactivity in the SX straight section. The goal of the next five years (until ∼2017) is to deliver a beam power greater than 100 kW, which would be the world's highest intensity for a slow extraction beam. In order to do this, we will have to gather experience and data about beam losses and residual activity through accelerator studies and user operational experience. If necessary, we will install local shields around the extraction devices for the reduction of residual activation. The new high repetition rate power supply is also expected to reduce current ripple by more than an order of magnitude, which will also improve the duty factor of the SX beam.

7. Summary

After the recovery from the earthquake, the MR restarted user operation in January 2012. The beam intensity has been gradually increased while carefully watching the beam losses and residual radioactivity of the accelerator components. The MR delivered a 200-kW beam to the T2K experiment and a 6-kW beam to particle and nuclear physics experiments in the hadron experimental hall until the summer shutdown of 2012. The beam intensity will be continuously increased by performing accelerator studies and hardware improvements. The goal of the next five years in the SX mode is to deliver a beam power larger than 100 kW to the hadron experimental hall. The designed beam power of 750 kW in the FX mode will be achieved by operation with a high repetition rate of ∼1 Hz. R&D projects for the main-magnet power supply and rf cavities required for such a high repetition rate scenario are now in progress.

Acknowledgements

We would like to thank all the members of the linac and the RCS for their outstanding efforts in delivering stable beams to us in the downstream facilities. We also thank the director of the Accelerator Laboratory of KEK, K. Oide, and project leaders in the construction and initial commissioning phase of the J-PARC accelerators, Y. Kamiya, H. Kobayashi, S. Nagamiya, F. Takasaki, A. Ando, Y. Yamazaki, and M. Yoshioka, for their advice and useful discussions during the beam commissioning and operation of the MR. Many other people whose names could not be listed here have contributed to the stable operation of the MR. Those people come not only from the KEK and JAEA institutions but also from cooperating companies, such as Mitsubishi Electric System Service, Nihon Advanced Technology, and others. We wish to express our sincere appreciation to all of them.

References

[1] Accelerator Group, JAERI/KEK Joint Project Team, "*Accelerator Technical Design Report for J-PARC*", KEK-Report 2002-13 and JAERI-Tech 2003-044.
[2] M. Yoshii, E. Ezura, K. Hara, K. Hasegawa, M. Nomura, C. Ohmori, A. Schnase, T. Shimada, A. Takagi, K. Takata, F. Tamura, M. Toda, and M. Yamamoto, Proc. IPAC 2011, p. 2502 (2011).

[3] M. Tomizawa, T. Adachi, Y. Arakaki, A. Ando, Y. Hashimoto, T. Koseki, H. Matsumoto, R. Muto, S. Murasugi, H. Nakagawa, J. Odagiri, K. Okamura, Y. Saito, K. Satou, Y. Shirakabe, H. Someya, J. Takano, S. Tokumoto, T. Toyama, and E. Yanaoka, submitted to Phys. Rev. ST.
[4] A. Molodozhentsev, T. Koseki, M. Shirakata, M. Tomizawa, and J. Yakano, Proc. IPAC 2010, p. 1937 (2010).
[5] K. Hasegawa, M. Kinsho, H. Oguri, and T. Koseki, Proc. IPAC 2011, p. 2727 (2011).
[6] M. J. Shirakata, Y. Fujii, T. Ishii, Y. Shirakabe, H. Harada, S. Harjo, T. Iwahashi, S. Meigo, T. Morishita, and N. Tani, Proc. IPAC 2011, p. 1662 (2011).
[7] T. Koseki et al., Proc. IPAC 2012, p. 3915 (2012).
[8] S. Igarashi, H. Harada, S. Hatakeyama, T. Koseki, M. Shirakata, J. Takano, F. Tamura, and T. Toyama, Proc. 8th Annual Meeting of PASJ, p. 324 (2011) [in Japanese].
[9] S. Igarashi, A. Ando, S. Hatakeyama, T. Koseki, Y. Sato, M. Shirakata, J. Takano, F. Tamura, and T. Toyama, Proc. 9th Annual Meeting of PASJ, WEPS015 (2012) [in Japanese].
[10] T. Koseki et al., Proc. HB2010, p. 16 (2010).
[11] Y. Kurimoto, M. Tobiyama, Y. Chin, T. Obina, T. Toyama, and Y. Shobuda, Proc. DIPAC2011, p. 482 (2011).
[12] K. Fan, H. Matsumoto, T. Sugimoto, S. Fukuoka, H. Someya, T. Toyama, and K. Ishii, Proc. IPAC 2012, p. 3728 (2012).
[13] T2K Collaboration, Phys. Rev. Lett. **107**, 041801 (2011).
[14] Y. H. Chin, Y. Kurimoto, T. Obina, M. Okada, K. Takata, M. Tobiyama, and Y. Shobuda, Proc. 9th Annual Meeting of PASJ, WELR09 (2012).
[15] F. Tamura, C. Ohmori, M. Yamamoto, M. Yoshii, A. Schnase, M. Nomura, M. Toda, T. Shimada, K. Hasegawa, and K. Hara, Phys. Rev. ST Accel. Beams **14**, 051004 (2011).
[16] S. Igarashi, Y. Hashimoto, K. Ohmi, K. Satou, Y. Sato, M. Shirakata, M. Tejima, and T. Toyama, Proc. IPAC 2011, p. 1239 (2011).
[17] T. Koseki et al., Proc. IPAC 2010, p. 1304 (2010).
[18] S. Igarashi, H. Someya, S. Nakamura, T. Oogoe, S. Yamada, and Y. Kuniyasu, Proc. IPAC 2010, p. 301 (2010).
[19] A. Schnase, F. Tamura, T. Koseki, M. Tomizawa, T. Toyama, M. Yoshii, C. Ohmori, M. Nomura, M. Yamamoto, M. Toda, H. Suzuki, T. Shimada, K. Hara, and K. Hasegawa, Proc. IPAC 2010, p. 1446 (2010).
[20] M. Tomizawa, M. Yoshizawa, K. Chida, J. Yoshizawa, Y. Arakaki, R. Nagai, A. Mizobuchi, A. Noda, K. Noda, M. Kanazawa, A. Ando, H. Muto, and T. Hattori, Nucl. Instrum. Methods Phys. Res., Sect. A **326**, 399 (1993).
[21] S. Nagamiya, Prog. Theor. Exp. Phys. **2012**, 02B001 (2012).
[22] K. Koseki, Y. Kurimoto, and Y. Morita, Proc. 9th Annual Meeting of PASJ, WEPS047 (2012) [in Japanese].
[23] C. Ohmori et al., Proc. IPAC 2011, p. 2885 (2011).